

Controlled Electron-Hole Trapping and Detrapping Process in GdAlO₃ by Valence Band Engineering

Luo, H; Bos, AJJ; Dorenbos, P

DOI

[10.1021/acs.jpcc.6b00129](https://doi.org/10.1021/acs.jpcc.6b00129)

Publication date

2016

Document Version

Accepted author manuscript

Published in

The Journal of Physical Chemistry C

Citation (APA)

Luo, H., Bos, AJJ., & Dorenbos, P. (2016). Controlled Electron-Hole Trapping and Detrapping Process in GdAlO₃ by Valence Band Engineering. *The Journal of Physical Chemistry C*, 120, 5916-5925. <https://doi.org/10.1021/acs.jpcc.6b00129>

Important note

To cite this publication, please use the final published version (if applicable). Please check the document version above.

Copyright

Other than for strictly personal use, it is not permitted to download, forward or distribute the text or part of it, without the consent of the author(s) and/or copyright holder(s), unless the work is under an open content license such as Creative Commons.

Takedown policy

Please contact us and provide details if you believe this document breaches copyrights. We will remove access to the work immediately and investigate your claim.

Controlled Electron-Hole Trapping and De-Trapping Process in GdAlO₃ by Valence Band Engineering

Hongde Luo, Adrie J.J Bos, Pieter Dorenbos*

Delft University of Technology, Faculty of Applied Sciences, Department of Radiation Science and Technology (FAME-RST), Mekelweg 15, 2629JB Delft, The Netherlands
E-mail: P.Dorenbos@tudelft.nl

Abstract:

Two different trapping and de-trapping processes of charge carriers have been investigated in GdAlO₃:Ce³⁺,Ln³⁺ (Ln= Pr, Er, Nd, Ho, Dy, Tm, Eu and Yb) and GdAlO₃:Ln³⁺,RE³⁺ (Ln=Sm, Eu and Yb, RE= Ce, Pr and Tb). Cerium is the recombination centre and lanthanide co-dopants act as electron trapping centres in GdAlO₃:Ce³⁺,Ln³⁺. Different lanthanide co-dopants generate different trap depths. The captured electrons released from the lanthanide recombine at cerium *via* the conduction band eventually producing the broad 5d-4f emission centred at ~360 nm from Ce³⁺. On the other hand, Sm³⁺, Eu³⁺ and Yb³⁺ act as recombination centres, while Ce³⁺, Pr³⁺ and Tb³⁺ act as hole trapping centres in GdAlO₃: Ln³⁺,RE³⁺. In this situation we find evidence that recombination is by means of hole release instead of the more commonly reported electron release. The trapped holes are released from Pr⁴⁺ or Tb⁴⁺ and recombine with the trapped electrons on Sm²⁺, Eu²⁺ or Yb²⁺ and yield characteristic trivalent emission from Sm³⁺, Eu³⁺ or Yb³⁺ at ~600 nm, ~617 nm or ~980 nm, respectively. Lanthanum was introduced to engineer the valence band energy and change the trap depth in Gd_{1-x}La_xAlO₃:Eu³⁺,Pr³⁺,Ln³⁺ and Gd_{1-x}La_xAlO₃:Eu³⁺,Tb³⁺. The results show that the valence band moves upwards and the trap depth related to Pr³⁺ or Tb³⁺ decreases.

Introduction:

The trapping and de-trapping processes of electrons and holes are of current interest due to the necessity to better understand the mechanism of afterglow and storage phosphors. An afterglow phosphor (or storage phosphor) is composed of the host lattice, the recombination (luminescence) centre and the trapping centre. The trapping centre can be either an electron or a hole trapping centre¹. For afterglow phosphors, the captured electrons/holes are spontaneously released at room temperature from the trapping centre and recombine in the luminescence centre, eventually causing emission that can range from UV to even near infrared depending on the luminescence centres and host lattices²⁻³. For storage phosphors, deeper traps are needed to prevent the thermal fading at room temperature⁴.

The electron trapping and de-trapping process has been widely investigated⁵⁻⁶. A good example is the well-known afterglow phosphor $\text{SrAl}_2\text{O}_4:\text{Eu}^{2+}, \text{Dy}^{3+}$. EXAFS confirmed that the concentration of trivalent europium increases after exposing the sample to UV light, indicating that Eu^{2+} is the electron donor and electrons are released due to photoionization⁷. The released electrons move freely in the conduction band and will be captured by the electron trapping centre. The nature of the trap is still under debate. The trapped electrons are released slowly and recombine with the europium recombination centre and eventually generates Eu^{2+} emission centred at $\sim 520 \text{ nm}$ ⁸. The trap depth in this case is the distance between the electron trapping level and the bottom of the conduction band (CB). The trap depth can be adjusted by the so-called band gap engineering technique. For example, Ga has been used to substitute Al in $\text{Gd}_3\text{Al}_{5-x}\text{Ga}_x\text{O}_{12}:\text{Cr}^{3+}, \text{Eu}^{3+9}$, $\text{Y}_3\text{Al}_{5-x}\text{Ga}_x\text{O}_{12}:\text{Ce}^{3+}, \text{Cr}^{3+5}$ and $\text{Zn}(\text{Ga}_{1-x}\text{Al}_x)_2\text{O}_4:\text{Cr}^{3+}, \text{Bi}^{3+10}$. It was claimed that substitution of Al by Ga lowers the CB that moves more close to the trapped electron level therefore decreasing the trap depth.

Instead of electrons being released from the electron trapping centre to recombine with a luminescence centre through the CB, holes can also be released from a hole trapping centre to recombine with a luminescence centre *via* the valence band (VB). However, rarely reports are published discussing about hole trapping and de-trapping processes. One of the few examples is $\text{MgS}:\text{Ce}^{3+}, \text{Sm}^{3+}$. Chakrabarti *et al* reported that samarium acts as a recombination centre and cerium as the trapping centre that capture holes after UV irradiation¹¹. The holes migrate from cerium to samarium producing Sm^{3+} characteristic emission during the TL readout. Similar phenomenon was also reported in $\text{YPO}_4:\text{Sm}^{3+}, \text{Tb}^{3+}$ by Bos *et al*¹². They observed that only Sm^{3+} characteristic emission in $\text{YPO}_4:\text{Sm}^{3+}, \text{Tb}^{3+}$ at 530 K during the TL readout, which indicates that holes are released from Tb^{4+} to recombine in the samarium luminescence centre.

The rare reporting on hole trapping and de-trapping processes is likely caused by a lack in our knowledge on how to identify a hole trapping centre and particularly on the depth of such trap. One needs knowledge on the location of the trapping levels with respect to the valence band maximum (VBM). One also needs to know whether the hole releases at lower temperature than the trapped electron. The knowledge on the energy at the VBM is also needed in other fields, for instance the “natural valence band offset” in semiconductor materials¹³⁻¹⁶ or for photocatalytic materials¹⁷. In those fields the VBM of a compounds is always specified with respect to that of another reference compound. It is not until 2012 that a model, called the chemical shift model, was developed to construct a Vacuum Referred Binding Energy (VRBE) diagram that makes it possible to compare the binding at the VB maximum in different compounds with respect to a same reference energy¹⁸⁻²⁰. A finding from this model is that the VRBE in the $4f^n$ ground state for lanthanides (both divalent and trivalent) is almost independent with type of compounds²¹⁻²⁴. Therefore, the lanthanide related hole trap depths can be adjusted by changing the VRBE at the top of the VB and electron trap depths by changing the VRBE at the bottom of the CB.

The objective of this study is to reveal electron and hole trapping and de-trapping processes. GdAlO_3 has been chosen as host lattice because of its simple structure with only one site to substitute for a trivalent lanthanide without the need for charge compensation²⁵. We prepared two groups of materials, one group is $\text{GdAlO}_3:\text{Ce}^{3+}, \text{Ln}^{3+}$ ($\text{Ln} = \text{Pr}, \text{Er}, \text{Nd}, \text{Ho}, \text{Dy}, \text{Tm}, \text{Eu}$ and Yb). Here Ce^{3+} will turn out to be the recombination and luminescence centre and the lanthanide co-dopants act as the electron

trapping centre with for each lanthanide a different trap depth. The other group is $\text{GdAlO}_3:\text{Ln}^{3+},\text{RE}^{3+}$ ($\text{Ln}=\text{Sm}, \text{Eu}$ and Yb , $\text{RE}=\text{Ce}, \text{Pr}$ and Tb). Here Ln^{3+} ions appear to be the recombination and luminescence centres and RE^{3+} ions act as hole trapping centres. The holes release from the RE^{4+} and recombine with Ln^{2+} producing Ln^{3+} emission *via* the VB. The trap depth of Pr and Tb can be adjusted by VB engineering techniques. Substitution of Gd by La will decrease the band gap but moves the absolute position of the valence band energy upwards, therefore the trap depths related to Pr and Tb hole trapping centres decrease.

2. Experimental

All starting materials were purchased from Sigma-Aldrich and used without further treatment. The appropriate stoichiometric mixture of Al_2O_3 (99.99%) and rare earth oxides with the purity of 5N (99.999%) were weighted according to the chemical formula and milled homogeneously with the help of acetone. After drying, the powder was synthesized at 1500°C for 10 h in a corundum crucible with the atmosphere of N_2/H_2 ($\text{N}_2:93\%,\text{H}_2:7\%$). After that, the obtained compounds were cooled down to room temperature.

All powders were checked with a PANalytical XPert PRO X-ray diffraction system with Co $K\alpha$ ($\lambda = 0.178901$ nm) x-ray tube (45 kV, 40 mA). The photoluminescence excitation (PLE) and photoluminescence emission (PL) measurement were measured with a set-up that consists of an UV/VIS branch with a 500W Hamamatsu CW Xe lamp and Gemini 180 monochromator and a VUV/UV branch using a deuterium lamp with an ARC VM502 vacuum monochromator. The Perkin Elmer MP-1913 photomultiplier was exploited as a detector connected at the exit slit of a Princeton Acton SP2300 monochromator. The sample is placed in an evacuated sample chamber.

TL measurements above room temperature (300-600 K) were performed with a RISØ TL/OSL reader model DA-15 and a controller model DA-20. Samples were irradiated with a $^{90}\text{Sr}/^{90}\text{Y}$ beta source with a dose rate of 0.7 mGy s^{-1} . Low temperature TL measurements (90-450 K) were recorded with a sample chamber operating under vacuum ($P = 10^{-7}$ mbar), a $^{90}\text{Sr}/^{90}\text{Y}$ beta irradiation source having a dose rate of ~ 0.4 mGy s^{-1} and a Perkin-Elmer channel PM tube (MP-1393). Liquid nitrogen was used as a cooling medium. A 3 mm C5-58 filter from about 350 to 470 nm was placed between the sample and PMT during the measurements of $\text{GdAlO}_3:\text{Ce}^{3+},\text{Ln}^{3+}$ ($\text{Ln}=\text{Pr}, \text{Er}, \text{Nd}, \text{Ho}, \text{Dy}, \text{Tm}, \text{Eu}$ and Yb). For the measurements of $\text{GdAlO}_3:\text{Ln}^{3+},\text{RE}^{3+}$ ($\text{Ln}=\text{Sm}, \text{Eu}$ and Yb , $\text{RE}=\text{Ce}, \text{Pr}$ and Tb), a 600 nm bandpass filter (600FS40-50) was placed between the sample and PMT²⁶.

TL emission spectra (TLEM) were measured using an UV to VIS spectrometer (Ocean Optics, QE65000) and a NIR spectrometer (Ocean Optics, NIRQ512) with a HR composite grating (300 lines/mm) and an entrance aperture of 100 mm resulting in a 3.3 nm (FWHM) wavelength resolution. The spectral range is 200 to 900 nm for QE65000 and 900 to 1700 nm for NIRQ512.

The TL excitation spectra (TLE) were measured by first illuminating the samples during 600 s with a monochromatic photon beam produced with a 150 W Xenon arc lamp (Hamamatsu L2273) filtered by a 1/8 monochromator (Oriel Cornerstone 130) with wavelength resolution of 0.8 nm/0.1 mm slit width. Next, the system is programmed to record all the TL glow curves from room temperature to 350°C with changing illumination wavelength. The plot of the integrated TL glow peaks versus the illumination wavelength is called a TL excitation spectra. A 600 nm bandpass filter (600FS40-50) was placed between the sample and PMT.

3. Results

3.1 X-Ray diffraction spectra, photoluminescence spectroscopy and vacuum referred binding energy diagram of GdAlO_3

Fig. 1 shows XRD patterns of GdAlO_3 with different content of lanthanum. The peaks of the synthesized phosphors exhibit a slight shift toward smaller 2θ angles with respect to the pattern of pure GdAlO_3 . This confirms that the lanthanum ions enter into the gadolinium site and increase the cell volume because lanthanum has larger ionic radius than gadolinium. A solid solution can be achieved provided that the La content remains less than 0.5. Two separate phases of GdAlO_3 and LaAlO_3 appear when the content of La is 0.75 (Fig. S1 in the Supporting Information).

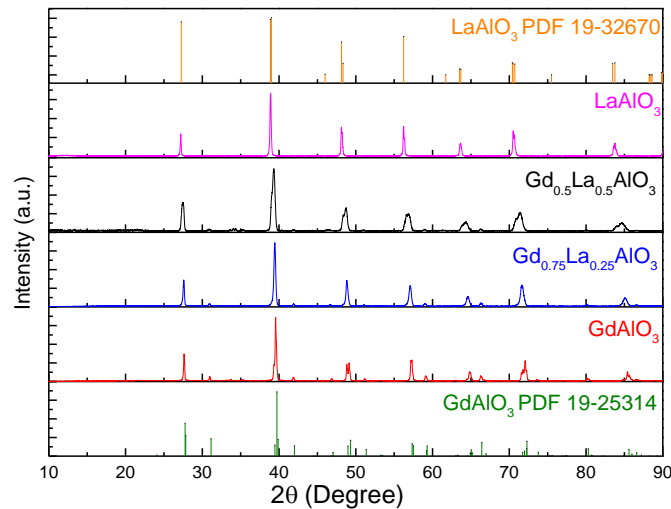


Fig. 1 XRD patterns of the as-prepared samples of GdAlO_3 , $\text{Gd}_{0.75}\text{La}_{0.25}\text{AlO}_3$, $\text{Gd}_{0.5}\text{La}_{0.5}\text{AlO}_3$ and LaAlO_3 .

Fig. 2 shows low temperature excitation and emission spectra of Eu^{3+} for different values of the La fraction x . The host exciton creation band can be observed in the VUV and decreased from 7.29 eV (170 nm) for GdAlO_3 to 6.38 eV (195 nm) for LaAlO_3 , which implies that the band gap decreases with increasing lanthanum content. The exciton energy found for GdAlO_3 and LaAlO_3 is close to values in previous reports, i.e., 7.08 eV (175 nm) for GdAlO_3 ²⁷ and 5.5 (225 nm)-6.5 eV (190 nm) for LaAlO_3 ²⁸⁻³¹. The broad excitation band in the UV between 200 nm and 290 nm for GdAlO_3 is due to electron transfer from the valence band to Eu^{3+} . It shifts towards longer wavelength with increase of x . The energy of the charge transfer band for Eu^{3+} decreases from 4.86 eV (255 nm) for GdAlO_3 to 3.93 eV (315 nm) for LaAlO_3 . The values are similar with those in previous reports: e.g., 4.68 eV (265 nm) for GdAlO_3 and 3.95 eV (314 nm) for LaAlO_3 ³². Fig. 2(b) shows the emission spectra of Eu^{3+} in $\text{Gd}_{1-x}\text{La}_x\text{AlO}_3$ with different content of La excited at the peak of the charge transfer band. All the samples show Eu^{3+} characteristic red emission.

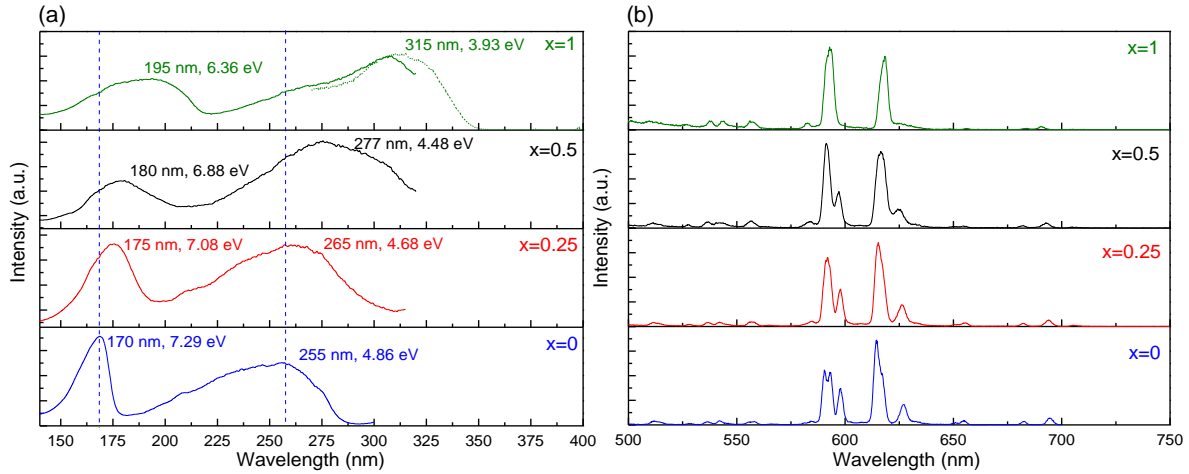


Fig. 2 PLE (a) and PL spectra (b) of $\text{Gd}_{1-x}\text{La}_x\text{AlO}_3:0.01\text{Eu}^{3+},0.01\text{Tb}^{3+}$ ($x=0, 0.25, 0.5$ and 1). The excitation spectrum from 150 to 320 was measured by deuterium lamp excitation (solid line). The excitation spectrum from 250 nm to 400 nm was measured by Xe lamp excitation (dotted line). The excitation spectra were recorded at 592 nm emission and the emission spectra were excited at the charge transfer peak maxima. All measurements were performed at 10 K.

Fig. 3 displays the vacuum referred binding energy (VRBE) scheme for GdAlO_3 . The zigzag curves labelled curve 1 and curve 2 connect the VRBE of an electron in the lowest $4f^n$ levels of the trivalent and the divalent lanthanides, respectively. All those VRBEs are fully determined from knowledge on the Coulomb repulsion energy of $U(6,A)=6.75$ eV as provided in Ref ²². The Eu^{3+} charge transfer energy of 4.86 eV as obtained from Fig. 2(a) and indicated by arrow 2 in Fig. 3 provides then the VRBE $E_V = -8.80$ eV at the top of valence band. The mobility band gap E_{VC} , or the energy between the bottom of the CB and the top of the VB, is obtained from the host exciton creation energy of 7.29 eV (Fig. 2) and an estimated value for the exciton binding energy. For wide band gap compounds it is estimated around 8% of the exciton creation energy, resulting in $E_{VC} = 7.87$ eV.

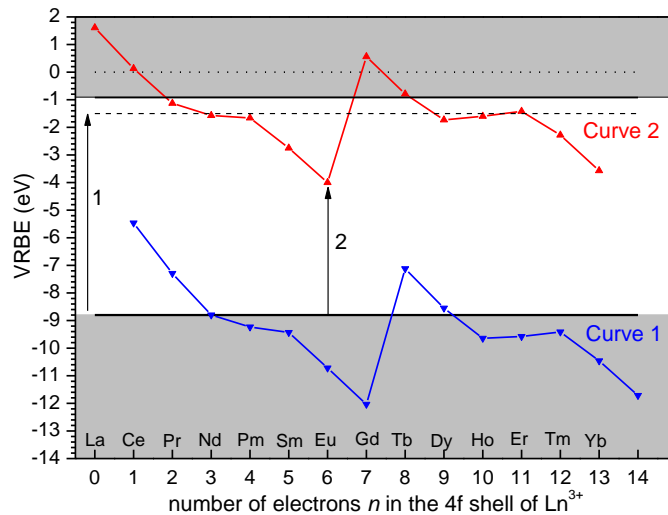


Fig. 3 Low temperature vacuum referred binding energy diagram for GdAlO_3 . Arrow 1 shows the transition of host exciton creation. Arrow 2 indicates the charge transfer from O^{2-} to Eu^{3+} .

The VRBE diagram predicts that electrons trapped by Pr^{3+} , Nd^{3+} , Sm^{3+} , Dy^{3+} , Ho^{3+} , Er^{3+} , Tm^{3+} or Yb^{3+} will be released at lower temperature than the holes trapped by Ce^{3+} and recombine with Ce producing Ce^{3+} 5d-4f emission. For combinations of $\text{Tb}^{3+}/\text{Pr}^{3+}$ with Sm^{3+} , Eu^{3+} or Yb^{3+} the scheme predicts that the holes release earlier from Tb^{4+} and Pr^{4+} than electrons from the deep traps by Sm, Eu, Yb to produce characteristic Sm^{3+} , Eu^{3+} , Yb^{3+} emission.

3.2 Thermoluminescence glow curves of GdAlO₃: Ce³⁺, Ln³⁺ (Ln= Pr, Er, Nd, Ho, Dy, Tm, Eu and Yb)

In Fig. 4 the normalised TL glow curves from Ce³⁺ 5d-4f emission in GdAlO₃:Ce³⁺, Ln³⁺ (Ln= Er, Nd, Ho, Dy and Tm) are shown. The TL maximum temperatures are spread out from 150 K for GdAlO₃:Ce³⁺,Er³⁺ to 413 K for GdAlO₃:Ce³⁺,Tm³⁺. No TL glow peaks with Ce³⁺ emission were observed for the samples co-doped with Pr³⁺, Sm³⁺, Eu³⁺ or Yb³⁺.

The trapping parameters of the Tm³⁺ trapping centre in GdAlO₃:Ce³⁺,Tm³⁺ were determined using the variable heating rate method^{5, 33-34} (Fig. S2). For the trap depth a value of 1.26 eV and for the frequency factor a value of 3x10¹⁴ s⁻¹ was found. Since all co-dopants Er³⁺, Nd³⁺, Ho³⁺, Dy³⁺ and Tm³⁺ replace Gd³⁺ in the host it is plausible to assume that the frequency factor remains the same³⁵. Then, the trap depths for the co-dopants Er³⁺, Nd³⁺, Ho³⁺, Dy³⁺ were found using the T_m from Fig. 4 and employing

$$\frac{\beta E}{kT_m^2} = s \exp\left(-\frac{E}{kT_m}\right) \quad (1)$$

where $\beta = 1\text{K s}^{-1}$ is the heating rate, k is the Boltzman constant (eV/K), $s = 3 \times 10^{14} \text{ s}^{-1}$, and T_m is the temperature (K) at the glow curve peak maximum. The values of the trap depths are shown in the legend of the figure.

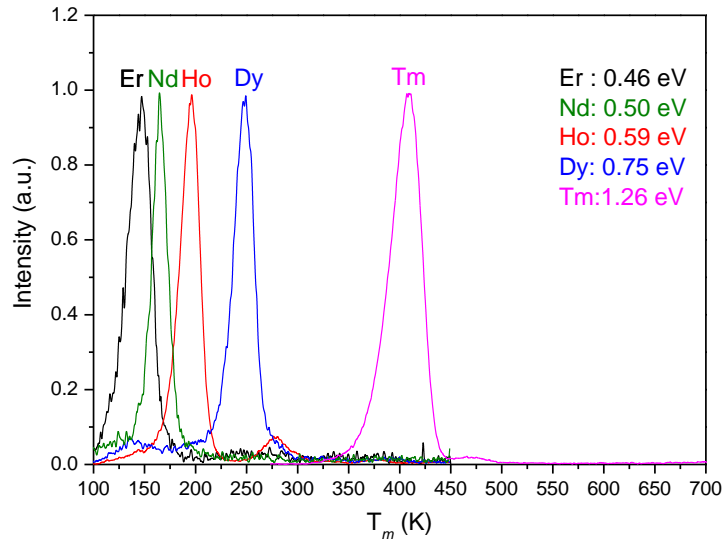


Fig. 4 Normalized thermoluminescence glow curves of GdAlO₃:0.01Ce³⁺,0.01Ln³⁺ (Ln= Er, Nd, Ho, Dy and Tm). The glow curves of Er, Nd, Ho and Dy co-doped samples were measured by the low-temperature TL setup from 90 to 450 K after 1600 s irradiation by its β source. GdAlO₃:Ce³⁺,Tm³⁺ was recorded by the RISØ TL-reader from 300 to 700 K after 1600 s irradiation by its β source. The heating rate was 1 K/s for all TL-recordings. The TL glow curves were measured with a Hoya 3 mm C5-58 bandpass filter from about 350 to 470 nm to transmit the 5d-4f Ce³⁺ emission (at 343 nm and 362 nm).

3.3 Thermoluminescence properties of GdAlO₃:Ln³⁺, RE³⁺ (Ln=Sm, Eu and Yb, RE= Ce, Pr and Tb) and Gd_{1-x}La_xAlO₃:Ln³⁺, Eu³⁺ (Ln= Sm and Eu).

Thermoluminescence emission (TLEM) spectra were measured for GdAlO₃:Ln³⁺, RE³⁺ (Ln=Sm, Eu and Yb, RE= Ce, Pr and Tb) samples in order to identify the luminescence and recombination centre during TL read-out. Fig. 5(a), (b) and (c) show typical TLEM spectra of GdAlO₃:Eu³⁺,Tb³⁺, GdAlO₃:Sm³⁺,Tb³⁺ and GdAlO₃:Yb³⁺,Tb³⁺. Similar figures for other dopant combinations can be found in Fig. S3.

Characteristic red Eu³⁺ emission with the associated TL glow curve centred at ~460 K (heating rate 5 K/s) can be observed for GdAlO₃:Eu³⁺ (Fig. S3(a)), GdAlO₃:Eu³⁺,Tb³⁺ (Fig. 5(a)), GdAlO₃:Eu³⁺,Pr³⁺

(Fig. S3(b)) and for $\text{GdAlO}_3:\text{Eu}^{3+},\text{Ce}^{3+}$ (Fig. S3(c)) samples. This glow peak will be referred to as peak 2 and will later be attributed to hole release from a host related defect. No emission from Tb^{3+} , Pr^{3+} or Ce^{3+} is observed indicating that only the Eu^{3+} ions act as the recombination (luminescence) centre in these samples. An additional shoulder (peak 4) in the TL-glow is observed at ~ 435 K in the $\text{GdAlO}_3:\text{Eu}^{3+},\text{Tb}^{3+}$ sample (Fig. 5(a)). For the $\text{GdAlO}_3:\text{Eu}^{3+},\text{Pr}^{3+}$ sample, the shoulder (peak 3) is at 15 K higher temperature ~ 450 K (Fig. S3(b)).

Similarly, a characteristic emission from Sm^{3+} with again the TL glow peak 2 centred at ~ 460 K is observed in $\text{GdAlO}_3:\text{Sm}^{3+}$ (Fig. S3(d)), $\text{GdAlO}_3:\text{Sm}^{3+},\text{Tb}^{3+}$ (Fig. 5(b)), $\text{GdAlO}_3:\text{Sm}^{3+},\text{Pr}^{3+}$ (Fig. S3(e)) and $\text{GdAlO}_3:\text{Sm}^{3+},\text{Ce}^{3+}$ (Fig. S3(f)) samples. Again no emission from Tb^{3+} , Pr^{3+} or Ce^{3+} is monitored. For $\text{GdAlO}_3:\text{Sm}^{3+},\text{Tb}^{3+}$ the shoulder peak 4 at ~ 435 K appears in Fig. 5(b). A similar shoulder peak 3 at ~ 445 K is observed for $\text{GdAlO}_3:\text{Sm}^{3+},\text{Pr}^{3+}$ in Fig. S3(e).

The Yb^{3+} characteristic emission from the ${}^2\text{F}_{7/2}$ level to the ${}^2\text{F}_{5/2}$ ground state is centred at ~ 980 nm and is observed both in $\text{GdAlO}_3:\text{Yb}^{3+}$ (Fig. S3(g)) and $\text{GdAlO}_3:\text{Yb}^{3+},\text{Tb}^{3+}$ (Fig. 5(c)). The glow peak 2 for both samples are found at ~ 460 K (heating rate 5 K/s). The $\text{GdAlO}_3:\text{Yb}^{3+},\text{Tb}^{3+}$ sample (Fig. 5(c)) shows a glow peak 4 at ~ 445 K, which is the same as those in Fig. 5(a) and Fig. 5(b). Yb^{3+} emission is absent in the $\text{GdAlO}_3:\text{Yb}^{3+},\text{Pr}^{3+}$ and $\text{GdAlO}_3:\text{Yb}^{3+},\text{Ce}^{3+}$ samples.

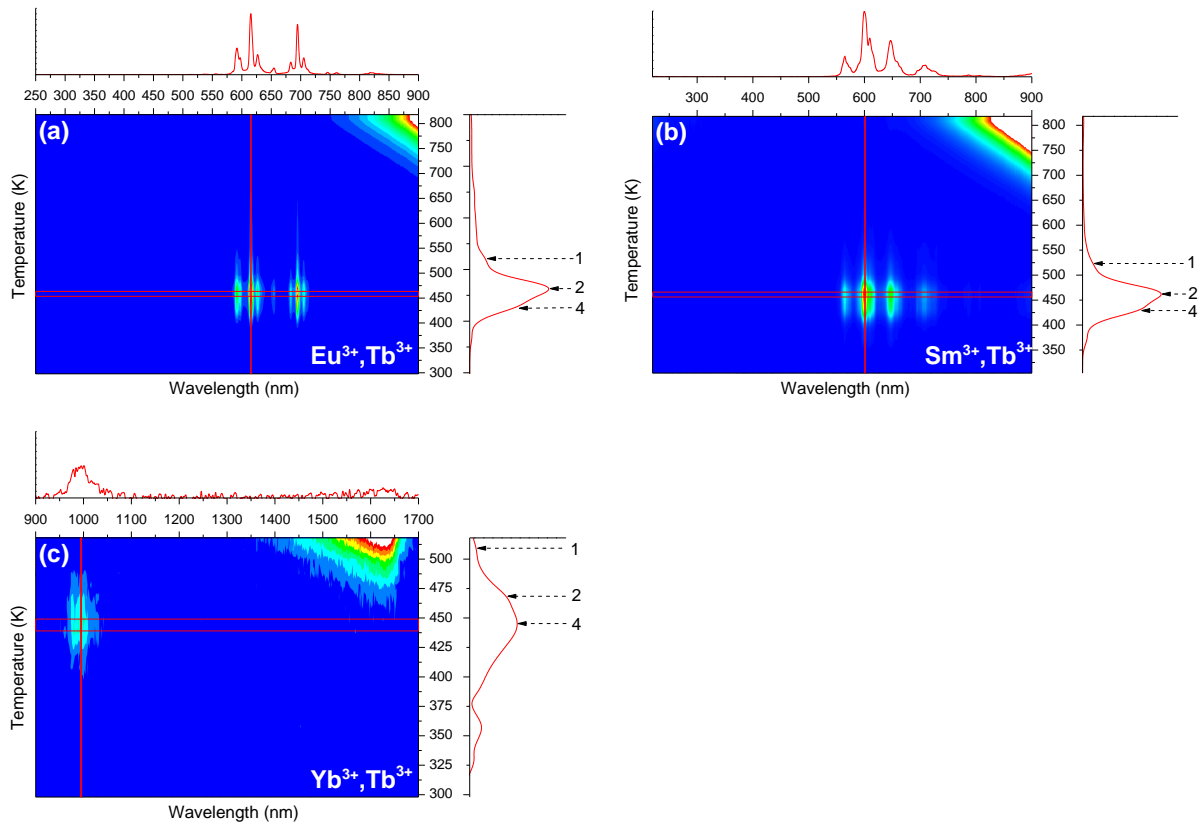


Fig. 5 The thermoluminescence emission (TLEM) spectra of (a) $\text{GdAlO}_3:0.01\text{Eu}^{3+},0.01\text{Tb}^{3+}$, (b) $\text{GdAlO}_3:0.01\text{Sm}^{3+},0.01\text{Tb}^{3+}$ and (c) $\text{GdAlO}_3:0.01\text{Yb}^{3+},0.01\text{Tb}^{3+}$. The samples (a) and (b) were measured by the UV to VIS spectrometer (Ocean Optics, QE65000) from 300 to 800 K, sample (c) was measured by the NIR spectrometer (Ocean Optics, NIRQ512) from 300 to 520 K. The heating rate for all of these samples is 5 K/s after exposure to irradiation of 2.5 kGy from a ${}^{60}\text{Co}$ source.

Fig. 6(a) and (b) show TL glow curves of $\text{GdAlO}_3:\text{Eu}^{3+},\text{RE}^{3+}$ and $\text{GdAlO}_3:\text{Sm}^{3+},\text{RE}^{3+}$ (RE= Ce, Pr and Tb). All samples share the same glow peaks 5 and 2 at ~ 350 K and ~ 450 K and an additional one at ~ 510 K (heating rate 1 K/s) hereafter referred to as peak 1. Glow peaks 4 and 3 appear at ~ 415 K and ~ 430 K for $\text{GdAlO}_3:\text{Eu}^{3+},\text{Tb}^{3+}$ and $\text{GdAlO}_3:\text{Eu}^{3+},\text{Pr}^{3+}$ in Fig. 6(a), respectively. These two peaks can also be observed at ~ 420 K or ~ 430 K for the samples co-doped with Tb^{3+} or Pr^{3+} in Fig. 6(b). Peaks 2, 3, and 4 appear also in the TLEM spectra (Fig. 5) at somewhat different temperature because

of the different heating rate. We conclude that peak 1 and 2 are from host related hole traps, peak 3 from Pr^{4+} and peak 4 from the Tb^{4+} hole trapping centre. No additional TL peaks are observed for Ce^{3+} co-doped samples. The trap depths were calculated with Eq. (1) using a frequency factor of $3 \times 10^{14} \text{ s}^{-1}$. Peak temperatures T_m and calculated trap depths are listed in Table 1. Since the TL intensity of Eu^{3+} doped samples are about twice higher than that of Sm^{3+} doped ones, the studies presented below were focused on the Eu^{3+} doped samples.

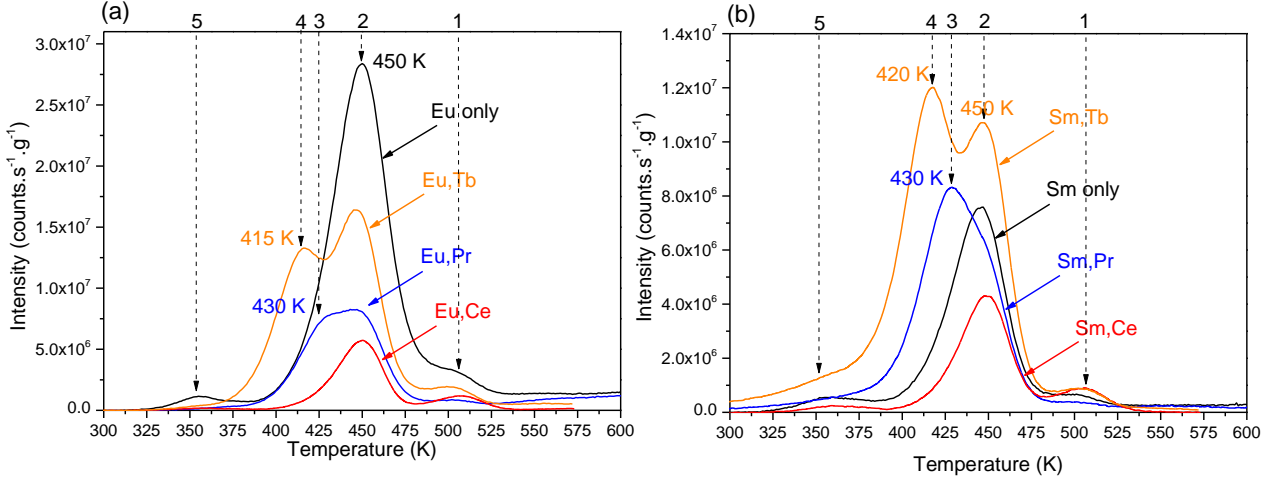


Fig. 6 Thermoluminescence glow curves of (a) $\text{GdAlO}_3:0.01\text{Eu}^{3+}, 0.01 \text{RE}^{3+}$, (b) $\text{GdAlO}_3:0.01\text{Sm}^{3+}, 0.01\text{RE}^{3+}$ ($\text{RE} = \text{Ce}, \text{Pr}$ and Tb). Fig. 6(a) and (b) were measured with the RISØ TL-reader from 300 to 600 K with 1600 s irradiation by its β source. The heating rate was 1 K/s for all TL-recordings. A 600 nm bandpass filter (600FS40-50) was placed between the samples and PMT. The peak intensities are calibrated by mass.

Table 1 List of samples, TL glow peaks and estimated trap depths

sample	glow peak	trap depth E (eV)
$\text{GdAlO}_3:\text{Eu}^{3+}$	2	1.39 ± 0.02
$\text{GdAlO}_3:\text{Eu}^{3+}, \text{Tb}^{3+}$	4 and 2	1.28 ± 0.02 and 1.39 ± 0.02
$\text{GdAlO}_3:\text{Eu}^{3+}, \text{Pr}^{3+}$	3 and 2	1.33 ± 0.03 and 1.39 ± 0.02
$\text{GdAlO}_3:\text{Eu}^{3+}, \text{Ce}^{3+}$	2	1.39 ± 0.02
$\text{GdAlO}_3:\text{Sm}^{3+}$	2	1.39 ± 0.02
$\text{GdAlO}_3:\text{Sm}^{3+}, \text{Tb}^{3+}$	4 and 2	1.29 ± 0.02 and 1.39 ± 0.02
$\text{GdAlO}_3:\text{Sm}^{3+}, \text{Pr}^{3+}$	3 and 2	1.33 ± 0.03 and 1.39 ± 0.02
$\text{GdAlO}_3:\text{Sm}^{3+}, \text{Ce}^{3+}$	2	1.39 ± 0.02

Fig. 7(a) shows the normalized TL glow curves for $\text{Gd}_{1-x}\text{La}_x\text{AlO}_3:\text{Eu}^{3+}, \text{Tb}^{3+}$ with different content of lanthanum. The as measured TL glow curves are shown in Fig. S4(a). One observes that the glow peak maxima shift towards lower temperature with increasing content of lanthanum. When the lanthanum content is 0.25 ($x=0.25$), peak 2 has weakened and shifted to 440 K. Peak 4 at 415 K for $x=0$ becomes much broader and shifts towards 390 K and 365 K for $x=0.25$ and 0.5, respectively. Peak 4 seems missing in the LaAlO_3 sample.

Our main conclusion is that peak 4 broadens and shifts towards lower temperature with increase of La concentration. The frequency factor for LaAlO_3 can be deduced as $6.5 \times 10^{13} \text{ s}^{-1}$ by the variable heating rate plot of $\text{LaAlO}_3:\text{Eu}^{3+}, \text{Tb}^{3+}$ (Fig. S5). However, the frequency factor for $x=0.25$ and 0.5 samples cannot be determined with this method because the TL glow peaks are much broadened. Considering that the compounds are quite similar, the frequency factor of $\text{Gd}_{1-x}\text{La}_x\text{AlO}_3$ for $x=0.25$ and 0.5 samples are fixed as $3 \times 10^{14} \text{ s}^{-1}$, sharing the same value of GdAlO_3 . The average traps depths are then estimated by Eq. (1) and the results are listed in Table 2 .

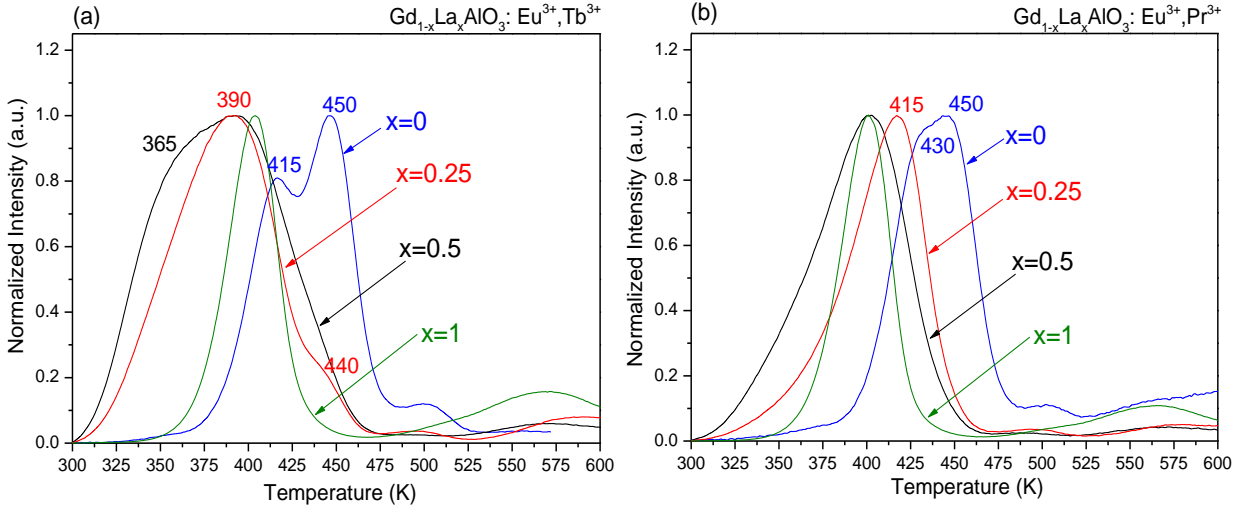


Fig. 7 Normalized thermoluminescence glow curves of (a) $\text{Gd}_{1-x}\text{La}_x\text{AlO}_3:0.01\text{Eu}^{3+},0.01\text{Tb}^{3+}$, (b) $\text{Gd}_{1-x}\text{La}_x\text{AlO}_3:0.01\text{Eu}^{3+},0.01\text{Pr}^{3+}$. All glow curves were measured by the RISØ TL-reader from 300 to 600 K with 1600 s irradiation by its β source. The heating rate was 1 K/s for all TL-recordings. A 600 nm bandpass filter (600FS40-50) was placed between the samples and PMT in order to select the Eu^{3+} emission.

Table 2 The glow peak positions and trap depths of $\text{Gd}_{1-x}\text{La}_x\text{AlO}_3:0.01\text{Eu}^{3+},0.01\text{Tb}^{3+}$.

x	peak position T_m (K)	trap depth E (eV)	frequency factor s (s^{-1})
0	415 ± 5 and 450 ± 5	1.28 ± 0.02 and 1.39 ± 0.02	3.0×10^{14}
0.25	390 ± 5 and 440 ± 5	1.20 ± 0.02 and 1.36 ± 0.02	(3.0×10^{14})
0.5	365 ± 15 and 395 ± 5	1.12 ± 0.05 and 1.22 ± 0.02	(3.0×10^{14})
1	400 ± 5	1.18 ± 0.02	6.5×10^{13}

Fig. 7(b) shows the normalized TL glow curves of $\text{Gd}_{1-x}\text{La}_x\text{AlO}_3:\text{Eu}^{3+}, \text{Pr}^{3+}$ with different content of lanthanum. The as measured TL glow curves are shown in Fig. S4(b). Similar to Fig. 7(a), the TL glow peaks below appear to shift to lower temperature when increasing the concentration of lanthanum. The clear double peak observed for $x=0$ is not observed for the La diluted samples. Trap depths are listed in Table 3.

Table 3 The peak positions and trap depths of $\text{Gd}_{1-x}\text{La}_x\text{AlO}_3:0.01\text{Eu}^{3+},0.01\text{Pr}^{3+}$.

x	peak positions T_m (K)	trap depths E (eV)	frequency factor s (s^{-1})
0	430 ± 10 and 450 ± 5	1.33 ± 0.03 and 1.39 ± 0.02	3.0×10^{14}
0.25	415 ± 5	1.28 ± 0.02	(3.0×10^{14})
0.5	400 ± 5	1.23 ± 0.02	(3.0×10^{14})
1	400 ± 5	1.18 ± 0.02	6.5×10^{13}

Figure 8(b) shows the Thermoluminescence excitation spectrum of $\text{LaAlO}_3:\text{Tb}^{3+} \text{Eu}^{3+}$. A broad band centred at ~ 315 nm is observed. For comparison the Eu^{3+} luminescence excitation spectrum from Fig. 2a is shown as well (Fig. 8(a)). The broad TLES band peaking at 315 nm corresponds with the broad CT-band also observed in the luminescence excitation spectrum.

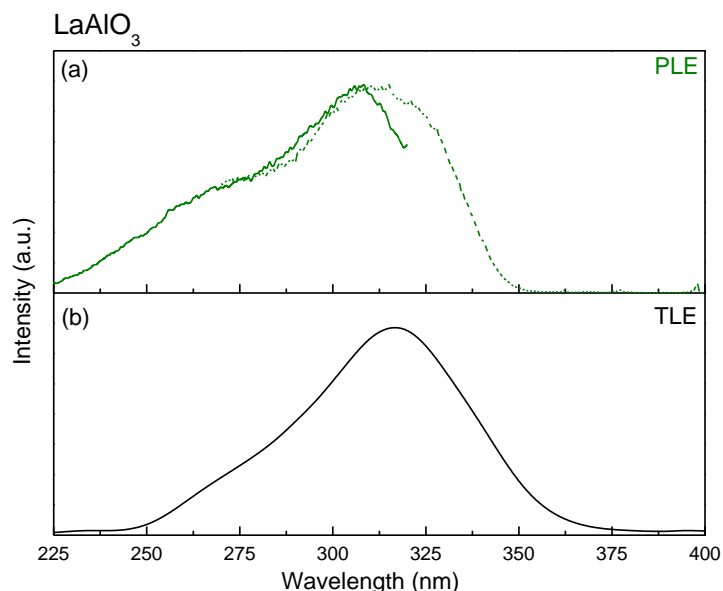


Fig. 8. The comparison of (a) photoluminescence excitation spectra of $\text{LaAlO}_3:0.01\text{Eu}^{3+}$ recorded at 592 nm emission and (b) thermoluminescence excitation spectrum of $\text{LaAlO}_3:0.01\text{Eu}^{3+},0.01\text{Tb}^{3+}$. The sample has been excited by a Xe lamp from 200 to 450 nm for 600 s before measuring. The thermoluminescence excitation spectra were obtained by plotting the integrated TL from 300 to 600 K as function of the excitation wavelength. The heating rate for TL readout is 1K/s and the wavelength step is 5 nm. The sample was illuminated at room temperature.

The iso-thermal decay spectra of $\text{Gd}_{1-x}\text{La}_x\text{AlO}_3:0.01\text{Eu}^{3+},0.01\text{Tb}^{3+}$ and $\text{Gd}_{1-x}\text{La}_x\text{AlO}_3:0.01\text{Eu}^{3+},0.01\text{Pr}^{3+}$ can be found in Fig. 9. The measurements were only carried out with the lanthanum content $x=0.25$ and 0.5 because these samples contain the significant tails at ~ 360 K that benefits to afterglow properties. One can observe that $\text{Gd}_{0.5}\text{La}_{0.5}\text{AlO}_3:0.01\text{Eu}^{3+},0.01\text{Tb}^{3+}$ has the best afterglow properties among all of the samples indicating a proper trap depth.

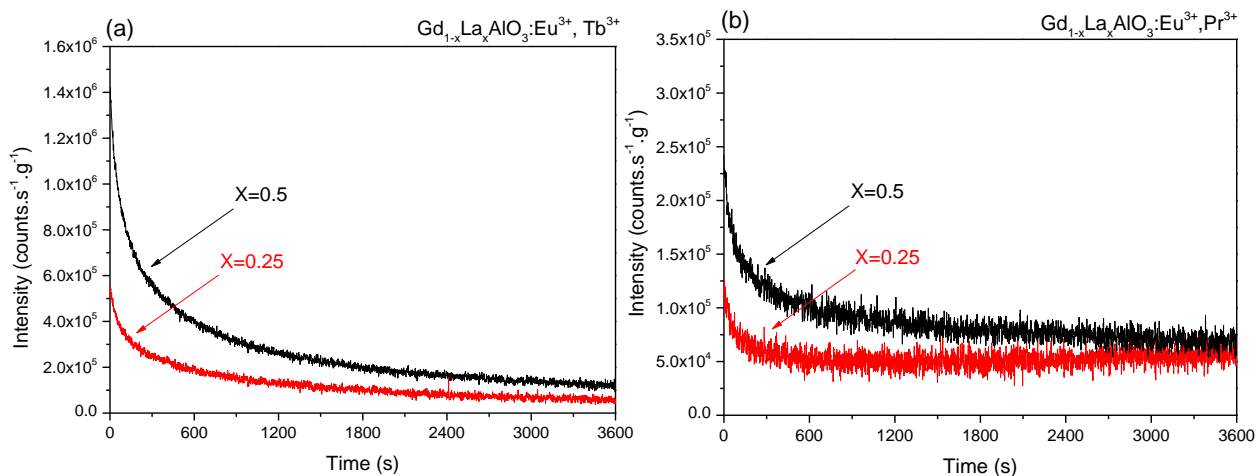


Fig. 9 The room temperature iso-thermal decay spectra of (a) $\text{Gd}_{1-x}\text{La}_x\text{AlO}_3:0.01\text{Eu}^{3+},0.01\text{Tb}^{3+}$, (b) $\text{Gd}_{1-x}\text{La}_x\text{AlO}_3:0.01\text{Eu}^{3+},0.01\text{Pr}^{3+}$ with $x=0.25$ and 0.5 . All the samples were irradiated by β source for 1600 s and the intensity was corrected by mass.

4. Discussion

To discuss the trapping and de-trapping process of charge carriers in GdAlO_3 , we will exploit the VRBE diagram in Fig. 3. The charge carriers generated by β irradiation can move freely through the conduction band and the valence band. Electrons are then trapped by electron trapping centres (like Nd, Sm, Dy, Ho, Er, Tm, Yb) and holes by hole trapping centres (like Ce, Pr, Tb). Such prediction of hole release, hole trapping and hole transport from a VRBE scheme (in contrast to the case of electrons) has never been really tested experimentally. Below we will provide evidence that the predictions fully agree with the observations. Note that holes tend to be shared between two oxygen anions to form a so-called V_k centre³⁶⁻³⁸. Often movement of such a centre is thermally activated and in a VRBE diagram one should place the V_k -hole state higher than above the top of the valence band with an amount equal to the binding energy of the V_k -centre³⁹.

A. Electron trapping and electron release

Fig. 4 shows that the TL glow peak temperatures T_m are different for different lanthanides in Ce^{3+} and Ln^{3+} ($\text{Ln} = \text{Er, Nd, Ho, Dy}$ and Tm) co-doped GdAlO_3 . The change in T_m implies that the type of lanthanide co-dopants influence the trap depth significantly.

In Fig. 10 the trap depths listed in the legend of Fig. 4 are compared with the VRBE levels in Fig. 3. They fully agree with the prediction made from the VRBE diagram however with a systematic shift. The diagram predicts that Tm has the deepest trap depth among the above five co-dopants (Er, Nd, Ho, Dy and Tm), resulting in its TL glow peak at the highest temperature. On the other hand, Er has the shallowest trap depth, which produces a TL glow peak at the lowest temperature. No TL glow peaks with Ce^{3+} emission can be found for (Ce,Pr), (Ce,Sm), (Ce,Eu) and (Ce,Yb) co-doped samples. The electron trap depth of Pr is predicted as very shallow and its glow peak temperature then will fall beyond the temperature range of our TL-facility. The trap depth of Sm^{2+} in the VRBE diagram is 1.83 eV which would correspond with $T_m = 587 \text{ K}$ if $s = 3.0 \times 10^{14} \text{ s}^{-1}$ and $\beta = 1 \text{ K/s}$. Ce^{3+} emission GdAlO_3 is totally quenched at this temperature²⁸. The trap depths of Eu^{2+} and Yb^{2+} are even deeper than that of Sm^{2+} and absence of Ce^{3+} TL-emission for these co-dopants is also attributed to thermal quenching of Ce^{3+} emission.

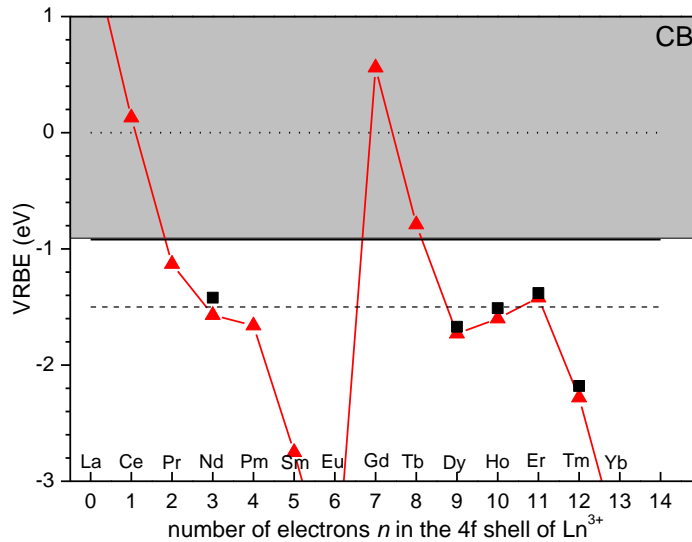


Fig. 10, Comparison of the VRBE predicted by the VRBE diagram (▲) and TL experiments (■)

Although the trap depths predicted by the VRBE diagram follow the values derived from the TL experiments there is one deviating data point. The VRBE diagram shows a trap depth of Nd^{2+} 0.03 eV deeper than that of Ho^{2+} . So one expects that the TL glow peak maximum temperature of Nd^{2+} is at a higher temperature than the one of Ho^{2+} . However, this is not the case (see Fig. 4). The same

phenomenon has been also found in TL glow curves in YPO_4 reported by Bos¹². This may indicate that the shape of curve 2 in Figure 2 needs a minor adjustment regarding the value for the ground state Nd^{2+} .

The agreement of the VRBE diagram prediction and TL experiments prove that indeed the Ln^{3+} ($\text{Ln} = \text{Er, Nd, Ho, Dy, and Tm}$) co-dopants are the electron trapping centres and Ce^{3+} is the recombination centre in $\text{GdAlO}_3:\text{Ce}^{3+}, \text{Ln}^{3+}$. During heating the electrons release from the lanthanide co-dopants and return through the conduction band to eventually recombine with Ce^{4+} producing emission from Ce^{3+} .

B. Hole trapping and hole release

In Fig. 5 a comparison was made of samples with the same hole trapping centre (Tb) but different electron trapping centres (Eu, Sm and Yb). All the samples show TL glow peaks at the same temperature (peak 1, peak 2 and peak 4 as assigned above) but with significantly different emission spectra. Peak 1 and 2 can be monitored in all the samples shown in Fig. 5, Fig. 6 and Fig. S3. Therefore, those peaks are assigned to an unidentified host related hole traps. Peak 4 appears only in the samples co-doped with Tb. The trap depth of peak 4 has been calculated as 1.28 ± 0.02 eV shown in Table 1. The estimated Eu^{2+} , Sm^{2+} and Yb^{2+} electron trap depths are 3.08 eV, 1.83 eV and 2.65 eV, thus much deeper than the trap depth for peak 4. The VRBE diagram predicts that the Tb^{3+} ground state is above the VB and Tb^{3+} may act as a hole trapping centre. During the TL readout, the activation energy needed to release holes from Tb^{4+} (1.28 ± 0.02 eV) is smaller than to release electrons from the electron trapping centres. Therefore, the holes release from Tb^{4+} earlier than electrons from Eu^{2+} , Sm^{2+} or Yb^{2+} producing characteristic Eu^{3+} , Sm^{3+} or Yb^{3+} 4f-4f emission.

A new peak (peak 3) appears in the Pr co-doped samples (Fig. 6). Again, no emission from Pr^{3+} can be found in the TLEM spectra shown in Fig. S3(b) and (e). This confirms that Pr^{3+} is not the recombination centre. The trap depth of peak 3 is 1.33 ± 0.03 eV as shown in Table 1, which is also much smaller than the electron trap depth of Eu^{2+} and Sm^{2+} . Considering that the ground state energy of Pr^{3+} and Tb^{3+} in the VRBE diagram is quite similar, also Pr^{3+} acts as the hole trapping centre. No Yb^{3+} emission was monitored in (Yb, Pr) co-doped sample. The explanation can be the energy transfer from $\text{Yb}^{3+} {}^2\text{F}_{7/2}$ to $\text{Pr}^{3+} {}^1\text{G}_4$ level that quenches the Yb^{3+} emission.

Ce^{3+} also acts as the hole-trapping centre according to the VRBE diagram. However, that trap is too deep to release a hole in the measurement range which explains that no TL extra peak(s) can be observed related to hole release from Ce^{4+} (Fig. 6, Fig. S3(c) and (f)).

The trap depth for Tb^{4+} and Pr^{4+} in Table 1 are 1.28 ± 0.02 eV and 1.33 ± 0.03 eV which are lower than predicted by the VRBE diagram (1.61 eV and 1.44 eV for Tb^{4+} and Pr^{4+}). The explanation can be that the released holes are not moving through the valence band but form a so-called V_k centre (a hole shared between two oxygen ions). The migration of a V_k centre is thermally activated and it will migrate to recombine at Eu^{2+} , Sm^{2+} or Yb^{2+} generating characteristic Eu^{3+} , Sm^{3+} or Yb^{3+} 4f-4f emission.

The thermoluminescence excitation (TLE) spectrum in Fig. 8 shows a broad band centred at ~ 315 nm which coincides with the Eu^{3+} CT-band in Fig. 2(a). During CT-band excitation electrons are excited from the valence band to the $\text{Eu}^{2+} 4f^7({}^8\text{S}_{7/2})$ ground state leaving a hole in the valence band. Those holes can be captured by Tb^{3+} to become Tb^{4+} . Some holes will be also captured by the host related hole trapping centre. In LaAlO_3 , Tb^{3+} will provide a very shallow hole trap depth, and they will be released immediately at room temperature. During the TL readout, the holes release from the hole trapping centres, forming the V_k centre and recombine with Eu^{2+} producing Eu^{3+} characteristic emission.

C. Engineering the trap depth by valence band tailoring

The above discussion of the hole trapping and hole release process confirms that the trap depths of the Tb^{3+} and Pr^{3+} hole trapping centres are related to the valence band maximum energy, indicating that the TL glow curves can be shifted by engineering the valence band.

Fig. 11 shows the VRBE diagrams for $Gd_{1-x}La_xAlO_3$ with different fraction of x . The data to construct the diagrams are listed in Table 4. The VRBE in the 4f ground state of Eu^{2+} ($E_{Eu^{2+}}$) is fixed at -3.98 eV because changes of $E_{Eu^{2+}}$ within the same type of compounds are insignificant. The charge transfer energy of Eu^{3+} in $Gd_{1-x}La_xAlO_3$ is shown in Fig. 2 and the detailed data are listed in Table 4. The decrease of the charge transfer energy of Eu^{3+} implies that the valence band maxima increases (Table 4). The ground state energy of Tb^{3+} and Pr^{3+} is like that for Eu^{2+} fixed for all the compounds.

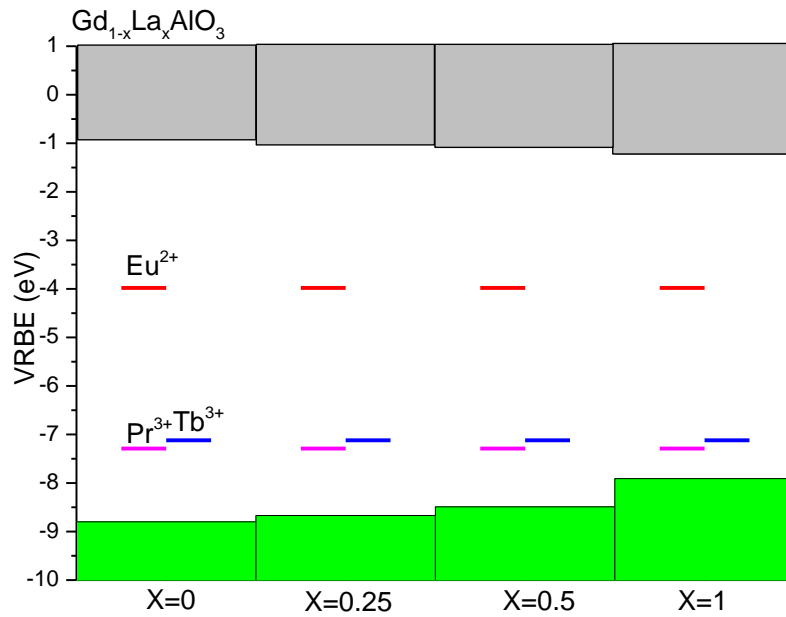


Fig. 11 VRBE diagram of $Gd_{1-x}La_xAlO_3$ ($x=0, 0.25, 0.5$ and 1)

Fig. 11 displays that the valence band goes upwards and the energy difference between Tb^{3+}/Pr^{3+} ground states and the valence band maxima decreases with increasing lanthanum concentration. The diagram agrees with the observed TL peak shift in Fig.7 where the Tb TL peak (peak 4) shifts from 415 ± 5 K (1.28 ± 0.02 eV) for $x=0$ to 365 ± 15 K (1.12 ± 0.05 eV) for $x=0.5$. A large uncertainty exists for $x=0.25$ and $x=0.5$ samples due to the very broad TL glow curves that make it tough to identify the exact TL peak maximum. The TL glow curves also shift to lower temperature with increasing lanthanum concentration in Fig. 7(b). However, the Pr TL peak can be only distinguished for $x=0$. The missing of peak 4 for $x=1$ ($LaAlO_3:Eu^{3+}, Tb^{3+}/Pr^{3+}$) is due to the very shallow hole trap depth in Pr^{4+} and Tb^{4+} creating a TL=peak far below the room temperature.

The ground state level of Pr^{3+} is ~ 0.17 eV lower than that of Tb^{3+} shown in the VRBE diagram indicating the TL glow peak maximum temperature of Pr^{3+} should be at a lower temperature than the one of Tb^{3+} . However, the TL experiments displays that the Pr TL peak (peak 3) T_m is ~ 10 K higher than that of the Tb peak (peak 4) shown in Fig. 6 and Table 1.

Table 4 The parameters to construct the VRBE diagram of $\text{Gd}_{1-x}\text{La}_x\text{AlO}_3:\text{Tb}^{3+}/\text{Pr}^{3+}$, Eu^{3+} ($x=0, 0.25, 0.5$ and 1). The units for all the parameters are all eV.

X	E^{ex}	E^{CT}	E_{V}	E_{C}	$E_{\text{Tb}^{3+}}$	$E_{\text{Pr}^{3+}}$
0	7.29	4.86	-8.80	-0.92	-7.12	-7.29
0.25	7.08	4.68	-8.67	-1.02	-7.12	-7.29
0.5	6.88	4.48	-8.49	-1.05	-7.12	-7.29
1	6.36	3.93	-7.91	-1.22	-7.12	-7.29

So far, we conclude that the trap depth of Tb hole trapping centres can be engineered by valence band tailoring with substitution of gadolinium by lanthanum.

5. Conclusion

The trapping and de-trapping process of electrons and holes have been studied in this paper. In $\text{GdAlO}_3:\text{Ce}^{3+}$, Ln^{3+} ($\text{Ln}=\text{Er, Nd, Ho, Dy}$ and Tm), the Ln^{3+} co-dopants are the electron trapping centres and Ce^{3+} is the hole trapping centre as well as the recombination centre. The captured electrons released from Ln^{2+} recombine with Ce^{4+} producing Ce^{3+} 5d-4f emission (at 343 nm and 362 nm). For $\text{GdAlO}_3:\text{Ln}^{3+}$, RE^{3+} ($\text{Ln}=\text{Sm, Eu}$ and Yb , $\text{RE}=\text{Ce, Pr}$ and Tb), the Ln^{3+} is the electron trapping centre as well as the recombination centre and RE^{3+} is the hole trapping centre. The holes release earlier (i.e. at lower temperature) than electrons and therefore recombine with Ln^{2+} generating Ln^{3+} 4f-4f characteristic emission during TL readout. The energy of the valence band maximum can be engineered by substitution of Gd by La therefore adjusting the trap depth of Tb^{3+} . Such valence band engineering may be a potential method to “deliberately design” the hole traps for afterglow phosphors.

6. Acknowledgements:

This research is supported by the Dutch Technology Foundation (STW), which is the applied science division of NWO, and the Technology program of the Ministry of Economic Affairs.

7. Supporting Information:

Including XRD; the Arrhenius plot of thermoluminescence (TL) with different heating rate; the thermoluminescence (TLEM) spectra and TL glow curves

Reference:

- (1). Aitasalo, T.; Hölsä, J.; Krupa, J. C.; Lastusaari, M.; Niittykoski, J., Persistent Luminescence Materials. *Physics of Laser Crystals*, Krupa, J.-C.; Kulagin, N., Eds. Springer Netherlands: 2003; Vol. 126, pp 35-50.
- (2). Van den Eeckhout, K.; Smet, P. F.; Poelman, D., Persistent Luminescence in Eu²⁺ Doped Compounds a Review. *Materials* **2010**, *3*, 2536-2566.
- (3). Van den Eeckhout, K.; Poelman, D.; Smet, P., Persistent Luminescence in Non-Eu²⁺-Doped Compounds: A Review. *Materials* **2013**, *6*, 2789-2818.
- (4). Leblans, P.; Vandenbroucke, D.; Willems, P., Storage Phosphors for Medical Imaging. *Materials* **2011**, *4*, 1034-1086.
- (5). Ueda, J.; Dorenbos, P.; Bos, A.; Kuroishi, K.; Tanabe, S., Control of Electron Transfer between Ce³⁺ and Cr³⁺ in Y₃Al₅-xGaxO₁₂ Host by Conduction Band Engineering. *J. Mater. Chem. C* **2015**, *3*, 5642-5651
- (6). Luo, H.; Bos, A. J. J.; Dobrowolska, A.; Dorenbos, P., Low-Temperature Vuv Photoluminescence and Thermoluminescence of Uv Excited Afterglow Phosphor Sr₃Al_xSi_{1-x}O₅:Ce³⁺,Ln³⁺ (Ln = Er, Nd, Sm, Dy and Tm). *Phys. Chem. Chem. Phys.* **2015**, *17*, 15419-15427.
- (7). Korthout, K.; Van den Eeckhout, K.; Botterman, J.; Nikitenko, S.; Poelman, D.; Smet, P. F., Luminescence and X-Ray Absorption Measurements of Persistent SrAl₂O₄:Eu,Dy Powders: Evidence for Valence State Changes. *Phys. Rev. B* **2011**, *84*, 085140.
- (8). Botterman, J.; Joos, J. J.; Smet, P. F., Trapping and Detrapping in SrAl₂O₄: Eu, Dy persistent phosphors: Persistent Phosphors: Influence of Excitation Wavelength and Temperature. *Phys. Rev. B* **2014**, *90*, 085147.
- (9). Xu, J.; Ueda, J.; Tanabe, S., Design of Deep-Red Persistent Phosphors of Gd₃Al₅-xGaxO₁₂:Cr³⁺ Transparent Ceramics Sensitized by Eu³⁺ as an Electron Trap Using Conduction Band Engineering. *Opt. Mater. Express.* **2015**, *5*, 963-968.
- (10). Zhuang, Y.; Ueda, J.; Tanabe, S., Tunable Trap Depth in Zn(Ga_{1-x}Al_x)₂O₄:Cr,Bi Red Persistent Phosphors: Considerations of High-Temperature Persistent Luminescence and Photostimulated Persistent Luminescence. *J. Mater. Chem. C* **2013**, *1*, 7849-7855.
- (11). Chakrabarti, K.; Mathur, V. K.; Rhodes, J. F.; Abbundi, R. J., Stimulated Luminescence in Rare Earth Doped Mgs. *J. Appl. Phys.* **1988**, *64*, 1363-1366.
- (12). Bos, A. J. J.; Dorenbos, P.; Bessière, A.; Lecointre, A.; Bedu, M.; Bettinelli, M.; Piccinelli, F., Study of TL Glow Curves of YPO₄ Double Doped with Lanthanide Ions. *Radiat. Meas.* **2011**, *46*, 1410-1416.
- (13). Kowalczyk, S. P.; Cheung, J. T.; Kraut, E. A.; Grant, R. W., CdTe-HgTe Heterojunction Valence-Band Discontinuity: A Common-Anion-Rule Contradiction. *Phys. Rev. Lett.* **1986**, *56*, (15), 1605-1608.
- (14). Wei, S.-H.; Zunger, A., Role of d orbitals in valence-band offsets of common-anion semiconductors. *Phys. Rev. Lett.* **1987**, *59*, (1), 144-147.
- (15). Li, Y.-H.; Walsh, A.; Chen, S.; Yin, W.-J.; Yang, J.-H.; Li, J.; Da Silva, J. L. F.; Gong, X. G.; Wei, S.-H., Revised Ab Initio Natural Band Offsets of All Group Iv, Ii-Vi, and Iii-V Semiconductors. *Appl. Phys. Lett.* **2009**, *94*, 212109.
- (16). Cai, Z.-H.; Narang, P.; Atwater, H. A.; Chen, S.; Duan, C.-G.; Zhu, Z.-Q.; Chu, J.-H., Cation-Mutation Design of Quaternary Nitride Semiconductors Lattice-Matched to Gan. *Chem. Mater.* **2015**, *27*, 7757-7764.
- (17). Xiaobo Chen, S. S., Liejin Guo, and Samuel S. Mao, Semiconductor-Based Photocatalytic Hydrogen Generation. *Chem. Rev.* **2010**, *110*, 6503-6570.
- (18). Dorenbos, P., Modeling the Chemical Shift of Lanthanide 4f Electron Binding Energies. *Phys. Rev. B* **2012**, *85*, 165107.
- (19). Dorenbos, P., Electronic Structure Engineering of Lanthanide Activated Materials. *J. Mater. Chem.* **2012**, *22*, 22344.
- (20). P.Dorenbos, A Review on How Lanthanide Impurity Levels Change with Chemistry and Structure of Inorganic Compounds. *ECS Journal of Solid State Science and Technology.* **2013**, *2*, (2), R3001-R3011.
- (21). Dorenbos, P.; Rogers, E. G., Vacuum Referred Binding Energies of the Lanthanides in Transition Metal Oxide Compounds. *ECS. J. Solid. State. Sc.* **2014**, *3*, R150-R158.
- (22). Dorenbos, P. The electronic level structure of lanthanide impurities in REPO₄, REBO₃, REAlO₃, and RE₂O₃ (RE = La, Gd, Y, Lu, Sc) compounds. *J. Phys: Condens Mat.* **2013**, *25*, (22), 225501.
- (23). Dorenbos, P., The Electronic Structure of Lanthanide Doped Compounds with 3d, 4d, 5d, or 6d Conduction Band States. *Journal of Luminescence* **2014**, *151*, 224-228.
- (24). Dorenbos, P., Lanthanide 4f Electron Binding Energies and the Nephelauxetic Effect in Wide Band Gap Compounds. *J. Lumin.* **2013**, *136*, 122-129.
- (25). du Boulay, D.; Ishizawa, N.; Maslen, E. N., GdAlO₃ Perovskite. *Acta. Crystallogr. C* **2004**, *60*, i120-i122.
- (26). Dobrowolska, A.; Bos, A. J. J.; Dorenbos, P., Electron Tunnelling Phenomena in YPO₄:Ce,Ln (Ln = Er, Ho, Nd, Dy). *J. Phys. D: Appl. Phys.* **2014**, *47*, 335301.

- (27). Verweij, J. W. M.; Cohen-Adad, M. T.; Bouttet, D.; Loutesse, H.; Moine, B.; Pédrini, C., Luminescence Properties of GdAlO₃: Ce Powders. Dependence on Reduction Conditions. *Chem. Phys. Lett.* **1995**, *239*, 51-55.
- (28). Lim, S.-G.; Kriventsov, S.; Jackson, T. N.; Haeni, J. H.; Schlom, D. G.; Balbashov, A. M.; Uecker, R.; Reiche, P.; Freeouf, J. L.; Lucovsky, G., Dielectric Functions and Optical Bandgaps of High-K Dielectrics for Metal-Oxide-Semiconductor Field-Effect Transistors by Far Ultraviolet Spectroscopic Ellipsometry. *J. Appl. Phys.* **2002**, *91*, 4500-4505.
- (29). Mi, Y. Y.; Yu, Z.; Wang, S. J.; Lim, P. C.; Foo, Y. L.; Huan, A. C. H.; Ong, C. K., Epitaxial LaAlO₃ Thin Film on Silicon: Structure and Electronic Properties. *Appl. Phys. Lett.* **2007**, *90*, 181925.
- (30). Edge, L. F.; Schlom, D. G.; Chambers, S. A.; Cicerella, E.; Freeouf, J. L.; Holländer, B.; Schubert, J., Measurement of the Band Offsets between Amorphous LaAlO₃ and Silicon. *Appl. Phys. Lett.* **2004**, *84*, 726-728.
- (31). Ohtomo, A.; Hwang, H. Y., A High-Mobility Electron Gas at the LaAlO₃/SrTiO₃ Heterointerface. *Nature* **2004**, *427*, 423-426.
- (32). Oliveira, H. H. S.; Cebim, M. A.; Da Silva, A. A.; Davolos, M. R., Structural and Optical Properties of GdAlO₃:RE³⁺ (RE = Eu or Tb) Prepared by the Pechini Method for Application as X-Ray Phosphors. *J. Alloy. Compd.* **2009**, *488*, 619-623.
- (33). Krumpel, A. H.; Bos, A. J. J.; Bessière, A.; van der Kolk, E.; Dorenbos, P., Controlled Electron and Hole Trapping in YPO₄: Ce³⁺, Ln³⁺ and LuPO₄: Ce³⁺, Ln³⁺ (Ln=Sm, Dy, Ho, Er, Tm). *Phys. Rev. B.* **2009**, *80*, 085103.
- (34). Azorín, J., Determination of Thermoluminescence Parameters from Glow Curves—I. A Review. *Int. J. Rad. Appl. Instrum. D* **1986**, *11*, 159-166.
- (35). Bos, A. J. J.; Dorenbos, P.; Bessière, A.; Viana, B., Lanthanide Energy Levels in YPO₄. *Radiat. Meas.* **2008**, *43*, 222-226.
- (36). Tasker, P. W.; Stoneham, A. M., An Appraisal of the Molecular Model for the V_k Centre. *J. Phys. Chem. Solids.* **1977**, *38*, 1185-1189.
- (37). Murray, R. B.; Keller, F. J., Recombination Luminescence from V_k Centers in Potassium Iodide. *Phys. Rev.* **1965**, *137*, A942-A948.
- (38). Gazzinelli, R.; Ribeiro, G. M.; de Siqueira, M. L., ESR and Endor Studies of the V_k Center in SrF₂. *Solid. State. Commun.* **1973**, *13*, 1131-1134.
- (39). Mott, N. F.; Stoneham, A. M., The Lifetime of Electrons, Holes and Excitons before Self-Trapping. *J. Phys. C : Solid. State. Phys.* **1977**, *10*, 3391.

Table of Contents Image

